PALEOCEANOGRAPHY, VOL. 28, 700–712, doi:10.1002/2013PA002541, 2013

Recovering the true size of an Eocene hyperthermal from the marine sedimentary record

Sandra Kirtland Turner[1,2] and Andy Ridgwell[2]

Received 1 August 2013; revised 17 October 2013; accepted 18 October 2013; published 9 December 2013.

[1] Hyperthermals—episodes of abrupt global warming associated with the massive injection of carbon into the oceans and atmosphere—represent possible analogs for future climate change. However, uncertainties in their magnitude, rate, and duration arising as a result of mixing processes and changes in carbonate preservation as the sediment record is formed complicate their use in constraining climate sensitivity and the role of carbon cycle feedbacks. Here, we use cGENIE, an Earth system model of intermediate complexity, to assess likely magnitude and rate of carbon input, taking a small hyperthermal event from the early-middle Eocene, C22nH3 (~49.2 Ma) as a case study. We develop an iterative method combined with a sediment model simulating the formation and mixing of deep-sea sediments to converge on an estimate for the "true" magnitude of the carbon cycle perturbation in the atmosphere and ocean that drives the event. In inverting the −0.95‰ benthic $\delta^{13}C$ excursion recorded at Ocean Drilling Program Site 1258, we obtain an estimate of at least −1.45‰ for the atmospheric CO_2 $\delta^{13}C$ excursion that drove event C22nH3. We also assess controls on intersite variation of event shape in model sediments and find that sedimentation rate is the strongest determinant of modeled event size, with higher sedimentation rate sites recording the atmospheric signal more accurately. Our revised estimate for the size of C22nH3 implies a total carbon input almost two-thirds higher than would be deduced if the recorded $\delta^{13}C$ excursion magnitude was taken at face value.

Citation: Kirtland Turner, S., and A. Ridgwell (2013), Recovering the true size of an Eocene hyperthermal from the marine sedimentary record, *Paleoceanography*, *28*, 700–712, doi:10.1002/2013PA002541.

1. Introduction

[2] Hyperthermals are events in the geologic record characterized by evidence for abrupt warming coupled with the release of massive quantities of isotopically depleted carbon to the oceans and atmosphere [*Thomas and Zachos*, 2000]. As such, they share many of the same key qualitative characteristics as modern anthropogenic carbon release [*Hönisch et al*., 2012] and could hence potentially provide important future insights. The Paleocene-Eocene Thermal Maximum (PETM, ~56 Ma) is the most widely studied hyperthermal event, but multiple purported hyperthermals occur throughout the surrounding greenhouse interval. A sequence of smaller hyperthermal events brackets the PETM from the late Paleocene to early Eocene (~58–53 Ma) [*Cramer et al*., 2003; *Lourens et al*., 2005; *Galeotti et al*., 2010; *Zachos et al*., 2010] with a number of similar events occurring near the early-middle Eocene transition (~48–50 Ma) [*Sexton et al*., 2011]. Distinguishing features of these events include a negative carbon isotope ($\delta^{13}C$) excursion recorded in marine and/or terrestrial sediments, evidence for warming, and dissolution of deep-sea carbonates [e.g., *Zachos et al*., 2005]. However, there is currently no agreement on the source of carbon responsible for these hyperthermals. Suggestions have included methane hydrates, permafrost carbon, dissolved marine organic carbon, and peat [*Kurtz et al*., 2003; *Higgins and Schrag*, 2006; *Lunt et al*., 2011; *DeConto et al*., 2012; *Sexton et al*., 2011; *Zachos et al*., 2010].

[3] In order to assess the carbon cycle and climate implications of hyperthermals and what (if any) future relevance they may have, it is necessary to determine the magnitude and rate of the carbon cycle perturbation. Unfortunately, the magnitude of the $\delta^{13}C$ excursions associated with hyperthermals is not unambiguously recorded. While records of the $\delta^{13}C$ change across the PETM exist from a variety of sources, including deep-sea and shallow marine carbonates and organic matter, soil carbonates, and terrestrial organic matter that together give us confidence that the perturbation to the carbon cycle is global, the excursion size varies widely between different sites and substrates (−1 to −6‰) [*Bowen et al*., 2004; *Panchuk*, 2007; *Dunkley Jones et al*., 2010; *Sluijs and Dickens*, 2012]. In general, marine organic carbon records show larger excursions than carbonate, with typical marine carbonate excursions being between −2 and −3.5‰ [*Nunes and Norris*, 2006; *Zachos et al*., 2007; *Panchuk*, 2007] compared to values as large as −6‰ in organic carbon [*Pagani et al*., 2006a,

Additional supporting information may be found in the online version of this article.

[1]Scripps Institution of Oceanography, University of California, San Diego, California, USA.
[2]School of Geographical Sciences, University of Bristol, Bristol, UK.

Corresponding author: S. Kirtland Turner, School of Geographical Sciences, University of Bristol, Bristol, BS8 1SS, UK. (ggxsk@bristol.ac.uk)

0883-8305/13/10.1002/2013PA002541

2006b; *Magioncalda et al*., 2004; *Cui et al*., 2011]. Because they are unattenuated by seafloor dissolution and bioturbation by deep-sea organisms, terrestrial records also typically show larger excursions compared to deep-sea records. However, organic carbon records are subject to uncertainty over potential changes in the composition of organic matter and the causes of fractionation in organic biomarkers [*Corsetti et al*., 2005; *Schouten et al*., 2007]. Additionally, changes in soil carbon dynamics, hydrology, and vegetation might amplify the excursion on land [*Bowen et al*., 2004; *Dunkley Jones et al*., 2010]. In the absence of any interpretative framework that can fully reconcile these varying recorded magnitudes, the size of the PETM carbon isotope excursion observed in well-preserved planktonic foraminifera (−4‰,) tends to be used as a surrogate for the excursion's true size [*Thomas et al*., 2002; *Zachos et al*., 2007; *Handley et al*., 2008; *John et al*., 2008; *Dunkley Jones et al*., 2010; *Cui et al*., 2011].

[4] Various model investigations of the potential causes and consequences of the perturbation to the carbon cycle and climate during the PETM have been made. They range in complexity from isotopic mass balance calculations [*Dickens et al*., 1995, 1997] to box models [*Kurtz et al*., 2003; *Zeebe and Zachos*, 2007; *Zeebe et al*., 2009] and to Earth system models which include climate feedbacks [*Panchuk et al*., 2008; *Cui et al*., 2011], but all work from an inferred size of the (global) carbon isotope excursion. However, even knowing the size of the carbon isotope excursion perfectly does not allow a unique solution to be obtained because different masses of carbon of varying isotopic composition could generate the same size excursion [*Dickens et al*., 1995; *Pagani et al*., 2006a]. Further constraints on the system are then needed. A release of carbon to the oceans-atmosphere will drive the ocean toward undersaturation (decreased carbonate ion concentrations) in some proportion to the quantity of carbon added, leading to a shoaling of the lysocline and carbonate compensation depth (CCD) [*Ridgwell and Zeebe*, 2005; *Kump et al*., 2009]. Assessing the decrease in carbonate preserved in deep-sea sediments across a hyperthermal then provides an additional constraint on the mass of the carbon pulse [*Zachos et al*., 2005; *Panchuk et al*., 2008; *Zeebe and Zachos*, 2007; *Zeebe et al*., 2009]. Models of the global carbon cycle thus need to include a representation of deep-sea sediments if they are to interpret the potential carbon release from both changes in carbonate preservation in marine sediments together with the carbon isotopic excursion. Modeling studies using this methodology suggest a total carbon input at the PETM of somewhere between 3000 and 6000 Pg C [*Panchuk et al*., 2008; *Zeebe et al.*, 2009].

[5] Successful elucidation of the magnitude and rate of carbon input underlying not only the PETM but also the various smaller hyperthermal events would allow improved comparisons to be drawn with future anthropogenic carbon release of how the impacts on climate, biogeochemistry, and ecosystem change scale with the forcing [e.g. *Gibbs et al*., 2012]. Most records of these Cenozoic hyperthermal events come from deep-sea carbonates [*Cramer et al*., 2003; *Lourens et al*., 2005; *Galeotti et al*., 2010; *Zachos et al*., 2010; *Sexton et al*., 2011]. The problem is that records are most likely compromised by a reduction in preservation or even chemical erosion of preexisting material. Bioturbation further complicates any simple interpretation of these records because the mixing process creates a strong filter on variations occurring in the ocean as a function of time [*Boudreau*, 1994; *Schiffelbein*, 1984], and it is the time variation in ocean properties predicted in models that is often used to contrast with geological observations.

[6] Here we utilize the coupled sediment model within the Earth system model "cGENIE" [*Ridgwell*, 2007a, 2007b] combined with deep-sea records of a relatively small but representative Paleogene hyperthermal to develop a method for estimating the true magnitude of the global carbon isotope excursion associated with the event. In other words, in this paper we will demonstrate how we can "recover" from the sedimentary archive the original, unmixed and unbiased by saturation change, global isotopic perturbation as a function of time. In recovering the underlying carbon isotope excursion, we also obtain estimates for the potential rate and magnitude of carbon input required to generate the event [e.g., *Panchuk et al*., 2008; *Cui et al*., 2011]. Our approach demonstrates the utility of simulating virtual sediment cores comparable to geologic data [*Ridgwell*, 2007a, 2007b; *Heinze*, 2001] and suggests a method for extracting additional information from biased proxy records of extreme climatic events like hyperthermals. We start the paper with an overview of the key components of the model that enables the numerical simulation of a deep-sea sediment record before summarizing the iterative inversion methodology (described in greater detail in Appendix A).

2. Methods

2.1. Model Description

[7] We employ cGENIE—an Earth system model that includes a 3-D dynamic ocean model with a simplified atmospheric energy-moisture balance plus sea-ice component, a representation of the biogeochemical cycling of a variety of elements and isotopes in the ocean [*Ridgwell et al*., 2007], and a spatially resolved sediment model [*Ridgwell and Hargreaves*, 2007] capable of generating virtual sediment "cores"—stacks of preserved deep-ocean sediments [*Ridgwell*, 2007a, 2007b]. The sediment model is paired with a simple weathering model [*Colbourn et al*., 2013] to provide long-term mass balance and feedback. The modern configuration of GENIE is capable of reproducing the observed large-scale distributions of nutrients [*Ridgwell et al*., 2007] and in the context of ocean carbon dynamics and isotopes, also of dissolved inorganic carbon $\delta^{13}C$ [*Holden et al*., 2013], and with projected anthropogenic ocean CO_2 and deep-ocean radiocarbon inventories close to data-based reconstructions [*Cao et al*., 2009]. The same model physics are applied to an early Eocene continental configuration and bathymetry (Figure 1a) in a configuration similar to that of *Ridgwell and Schmidt* [2010] and *Cui et al*. [2011]. In this, annual average surface ocean wind stress and wind speed together with zonally and annually averaged albedo are regridded from a $\times 3CO_2$ fully coupled general circulation model (GCM) Eocene simulation [*Tindall et al*., 2010]. A reduction in the solar constant of 0.46% and 1% decrease in mean ocean salinity (representing an ice-free world) are also applied.

[8] Also following *Ridgwell and Schmidt* [2010], we used the following initial carbon cycle conditions for the late Paleocene/early Eocene: 834 ppm atmospheric CO_2, $\delta^{13}C$ of atmospheric CO_2 of −4.9‰, Ca^{2+} of 18.22 mmol/kg, Mg^{2+}

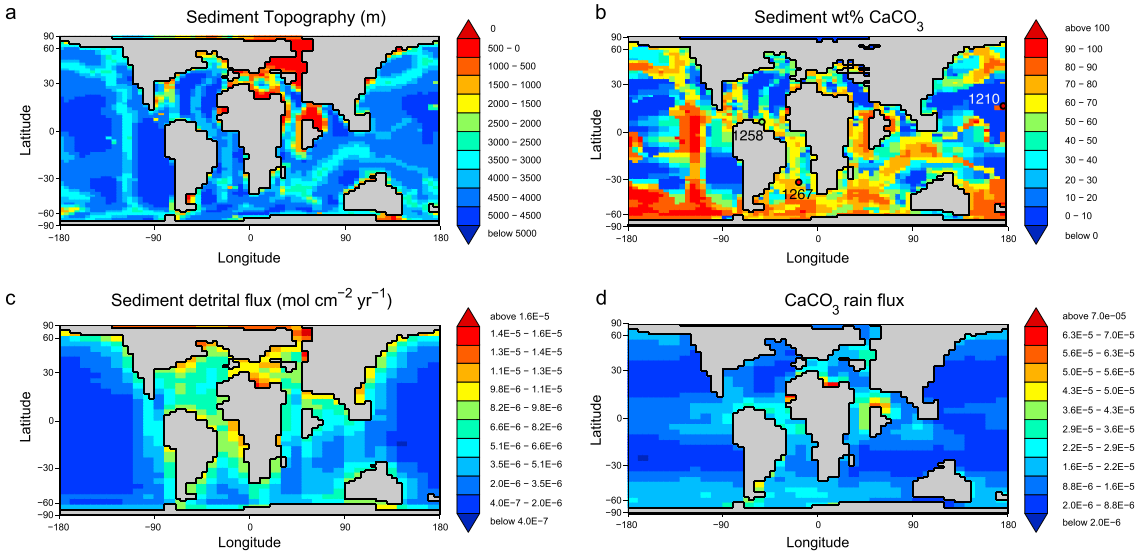

Figure 1. Initial conditions for cGENIE experiments: (a) sediment topography (m), (b) seafloor carbonate distribution with observations from three sites (selected to approximate ODP Site 1258 in the equatorial Atlantic, ODP Site 1267 in the South Atlantic, and ODP Site 1210 in the Central Pacific) superimposed, (c) detrital flux field, and (d) carbonate rain flux. Carbonate plus the detrital fraction is equal to 100% of sediment content.

of 29.89 mmol/kg, and SO_4^{2-} of 15 mmol/kg. We set global mean alkalinity in the ocean initially at 2075 µmol/kg, which results in a mean dissolved inorganic carbon (DIC) concentration of 2071 µmol/kg. This gives rise to a global deep-sea sediment burial rate of 14.5 Tmol $CaCO_3$/yr and mean surface sedimentary $CaCO_3$ content (below 176 m water depth) of 43.5 wt% (Figure 1b). Balancing sedimentary burial then constrains the weathering rate at 14.5 Tmol of $CaCO_3$ per year (and $\delta^{13}C$ of 2.0‰)—similar to the 17.5 Tmol yr^{-1} Ca^{2+} equivalent of *Panchuk et al*. [2008] and midway between the low and high estimates of *Cui et al*. [2011] but less than the elevated Eocene bicarbonate fluxes predicted in a paleo-GCM climate and land surface weathering modeling study [*Gibbs et al*., 1999]. All cGENIE experiments are initiated from a 50 kyr long model spin-up that equilibrates deep-sea sediment composition. In light of the relatively short duration of the event, no silicate-weathering feedback was included in these experiments.

2.2. Modeling of Eocene Deep-Sea Sediments

[9] The sediment model in cGENIE is important in this study because it can simulate the formation of stacked records of deep-sea sediment composition (virtual sediment cores) that we can directly compare to sediment core data [*Ridgwell*, 2007a, 2007b]. Carbonate reaching the seafloor can be buried or dissolved, according to fractional $CaCO_3$ preservation calculated in the carbonate diagenesis model of *Archer* [1991] [*Ridgwell*, 2007a]. In this model, any organic carbon that reaches the seafloor is assumed to be fully oxidized within the sediments, with the liberated metabolic CO_2 potentially available to drive pore water undersaturation and hence $CaCO_3$ dissolution. A spatially uniform ratio of carbonate to particulate organic carbon exported from the ocean surface is set, with a value (0.175) similar to values (0.200) used previously [*Panchuk et al*., 2008; *Ridgwell and Schmidt*, 2010]. This ratio is chosen to provide an approximate match between model and observed sedimentary wt% $CaCO_3$ at the three model sites evaluated in this study (Figures 1b and 1d). The prescribed detrital flux varies spatially according to a simple assumption of decay of flux with distance from the continents (Figure 1c) with the controlling *e*-folding distance adjusted to fit the reconstructed (late Paleocene) detrital accumulation rates given by *Zeebe and Zachos* [2007]. Additionally, we do not consider the cycle of opal here such that sediments can be composed only of carbonate and/or detrital material.

2.3. Simulation of Sediment Cores and the Role of Bioturbation

[10] Simulating the first-order controls on how the carbonate $\delta^{13}C$ signal is recorded in accumulating marine sediments is central to this study, so we provide a summery here (fuller details can be found in *Ridgwell* [2001, 2007a, 2007b] and see *Ridgwell* [2007a, Figure 1]). In the model, settling carbonate and detrital material at the ocean floor is first incorporated into a 1 cm thick surface layer where sediment mass balance (settling flux minus dissolution) is calculated. Excess accumulating material is deposited in a series of 1 cm thick layers in an underlying sediment stack. Episodes of chemical erosion of previously deposited carbonates are simulated by the removal of carbonate layers from the top of this stack.

[11] As carbonate is deposited to the sediments, it is tagged with an "age," with the resulting age of a sediment column layer being equal to the average age of the carbonate deposited to that layer [*Ridgwell*, 2007a]. This allows for the extraction of sediment core properties as a function of sediment age as well as depth below the sediment surface and hence facilitates assessment of the relative timing of signals recorded in sediments against changes occurring in the ocean and atmosphere. In addition to the preservation of bulk $CaCO_3$, which carries an isotopic signature closely related to the surface ocean via the inorganic $\delta^{13}C$ fractionation versus

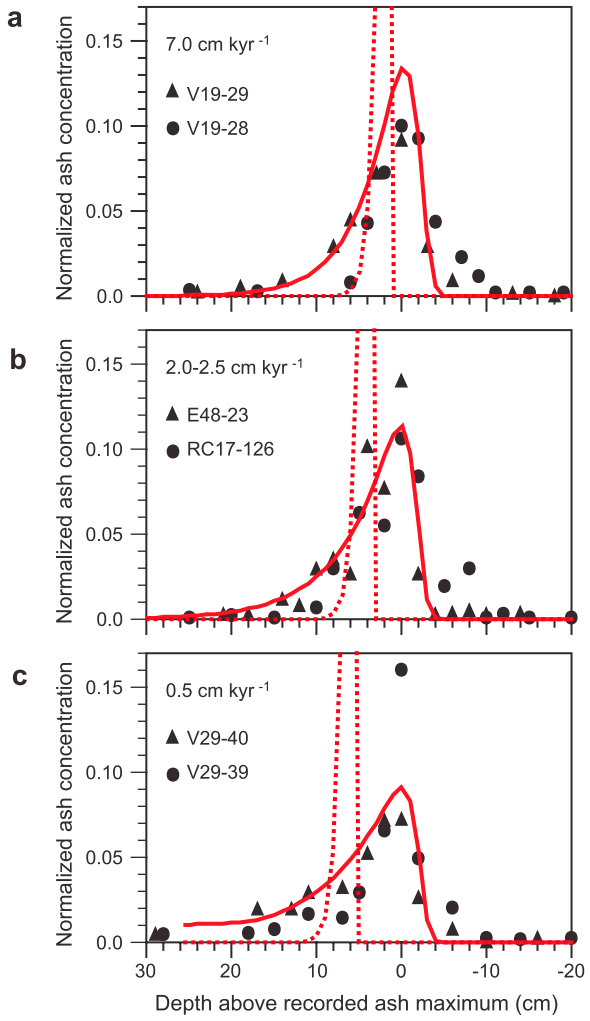

Figure 2. Simulation of bioturbational mixing of an impulse event. Predicted profiles of an impulse of ash applied to the sediment surface (solid red line) compared to observed ash and pumice profiles [*Ruddiman et al.*, 1980]. Both model and observed tracer concentrations are normalized to unit-integrated volume and their maximum concentrations aligned in depth (defined as 0 cm). In other words, zero depth is defined as the level at which the event apparently occurs and does not necessarily imply that this indicates when the volcanic event actually occurred. Also shown are predicted down-core ash profiles in the absence of bioturbation (dotted red line). In this case, the depth scale is exactly the same as for the simulation with bioturbation, and the simulation peak has not been realigned, illustrating the apparent shifting of an event by bioturbation. In the simulation without bioturbation, the presence of up-core decay in concentration profiles reflects the presence of some vertical numerical diffusion in the sediment model—i.e., the propagation of a small fraction of the signal upward in the absence of any physical mechanism by which this could occur. Simulations are shown for virtual sediment cores with (a) a 7.0 cm/kyr sedimentation rate, (b) a 2.0–2.5 cm/kyr sedimentation rate, and (c) a 0.5 cm/kyr sedimentation rate.

HCO_3^- of *Mook* [1986] (Figure 1d), we also include tracers reflecting planktonic and benthic foraminiferal $CaCO_3$. These additional tracers are created in proportion to bulk $CaCO_3$ but do not play any role in the global mass budget and as configured for this current study do not assume any fractionation between HCO_3^- and $CaCO_3$.

[12] Sediment mixing, by the feeding, burrowing, and locomotion activities of benthic animals, reduces the recorded magnitude and increases the apparent duration of a signal [e.g., *Schiffelbein*, 1984; *Trauth*, 1998]. To account for this, the sediment model applies a prescribed profile of mixing between the surface layer and uppermost layers in the sediment stack to simulate (1) a well-mixed 5 cm thick surface layer (high, uniform biodiffusion coefficient) and (2) deeper but less frequent bioturbation activity by means of a biodiffusion coefficient that decreases with depth with an *e*-folding length of 1 cm [*Ridgwell*, 2007a]. The maximum value of the biodiffusion coefficient in the surface layers ($16\,cm^2\ kyr^{-1}$) and the scale depth below this were determined by calibrating the biodiffusion coefficient to observed profiles of radiocarbon following *Peng et al.* [1979] [see *Ridgwell*, 2001]. This same mixing profile is applied to all sediment locations in the model, although in reality, the depth of mixing in marine sediments can be expected to vary as some function of the flux of particulate organic material to the seafloor [*Hull et al.*, 2011; *Smith and Rabouille*, 2002; *Trauth et al.*, 1997].

[13] Taking as an example the virtually instantaneous deposition of an easily identifiable material whose mass is conserved within the sediments (volcanic ash and pumice) [*Ruddiman et al.*, 1980], Figure 2 illustrates the effect of bioturbation in cGENIE and to what degree a simple biodiffusion profile can (or cannot) capture observed features of the marine geological record. Bioturbation reduces the recorded magnitude of the ash pulse and also shifts the apparent timing of the event, such that the pulse appears to occur earlier than in simulations made in the absence of bioturbation. The magnitude of both these effects increases with decreasing sedimentation rate. Overall, the choice of bioturbation magnitude and its distribution with depth results in a simulated ash profile that closely follows observations across a wide range of sediment accumulation rates, particularly for sediment depths above the event horizon. However, simple biodiffusion schemes as employed here fail to capture the effect of rare deep mixing events. This is apparent in the shorter tail below the event horizon simulated in the model compared to observations.

2.4. Model-Data (Inversion) Methodology

[14] Our primary data set is the benthic foraminiferal $\delta^{13}C$ record for event C22nH3 from *Sexton et al.* [2011], recorded at Demerara Rise in the equatorial Atlantic, Ocean Drilling Program (ODP) Site 1258. C22nH3 occurred at ~49.2 Ma and had an estimated duration of ~36 kyr if one defines the onset as the point at which $\delta^{13}C$ begins to decrease and the termination when $\delta^{13}C$ returns to a value approximately as heavy as the onset. ODP 1258 has a paleodepth for the Eocene of ~3000 m with pre-event wt% $CaCO_3$ of 52% and a sedimentation rate that reaches a maximum of 2–2.5 cm/kyr [*Sexton et al.*, 2006]. The $\delta^{13}C$ excursion recorded at ODP Site 1258 for C22nH3 has a magnitude of −0.95‰ with the $\delta^{13}C$ minimum occurring 15 kyr after the onset of the event. Sample spacing is 3–5 kyr with all ages determined from an astronomically tuned age model [*Sexton et al.*, 2011].

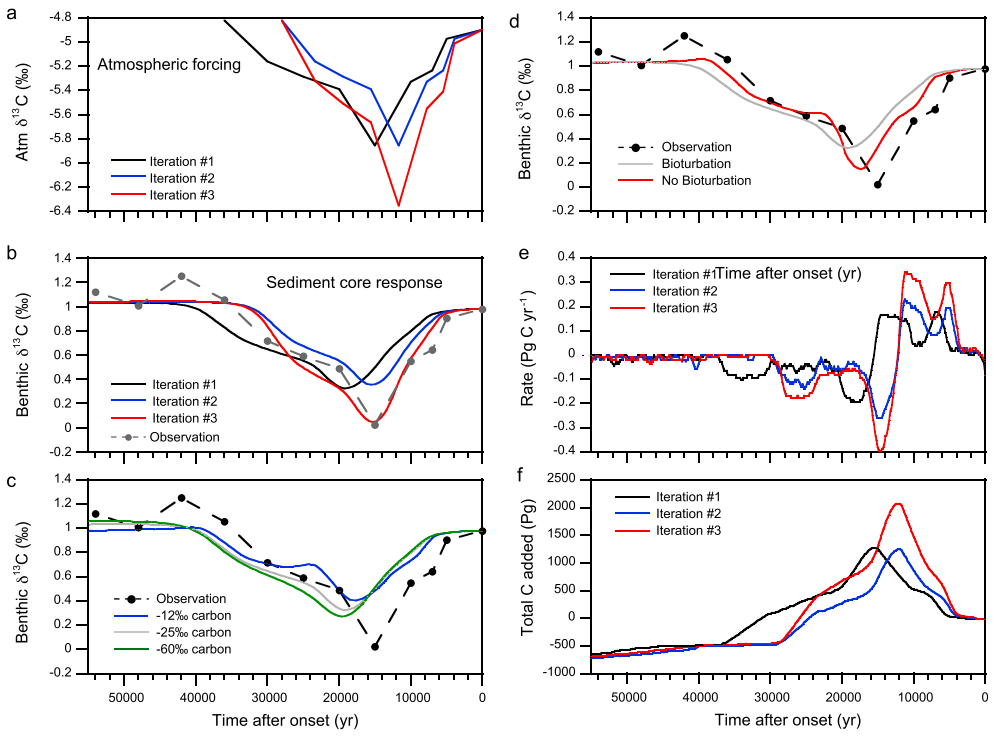

Figure 3. Results of inversion experiments: (a) Evolution of the applied atmospheric CO_2 $\delta^{13}C$ over three runs including the observational benthic foraminiferal CIE from ODP Site 1258 [*Sexton et al.*, 2011] adjusted to atmospheric values (i.e., relative to −4.9‰) applied as the forcing in Iteration #1 (black line), the forcing in Iteration #2 (blue line), and the forcing applied in Iteration #3—or the "backed out" CIE (red line). (b) Evolution of sediment core benthic foraminiferal $\delta^{13}C$ response at Site 1258′ to the atmospheric excursions applied in Figure 3a including the observational benthic foraminiferal $\delta^{13}C$ data with the starting value adjusted to the model-derived initial value of 0.977‰ (grey dashed line), the response to Iteration #1 (black line), the response to Iteration #2 (blue line), and the response to Iteration #3 (red line). (c) Comparison of model sediment core results for Site 1258′ when the excursion in Iteration #1 is applied to the atmosphere using carbon inputs of varying isotopic composition: −12‰ (blue line), −25‰ (grey line), and −60‰ (green line). Black dashed line indicates the CIE recorded in benthic foraminifera from ODP Site 1258. (d) Comparison of model sediment core results for the Site 1258′ when the excursion in Iteration #1 is applied to the atmosphere with bioturbation on (grey line) and bioturbation off (red line). In both cases, the applied carbon pulse has a $\delta^{13}C = -25‰$. (e) Diagnosed rate of carbon addition/removal in Pg yr^{-1} when forcing atmospheric CO_2 $\delta^{13}C$ to match the excursion in Iteration #1 (black line), the excursion in Iteration #2 (blue line), and the excursion in Iteration #3 (red line). (f) Total carbon added to generate the excursion in Iteration #1 (black line), the excursion in Iteration #2 (blue line), and the excursion in Iteration #3 (red line).

[15] We adapted the inversion method of *Cui et al.* [2011] in which isotopically depleted carbon was automatically and uniformly added or subtracted from the atmosphere such that the modeled atmospheric $\delta^{13}C$ tracked a prescribed curve. Our particular advance here is to repeat the inversion iteratively, adjusting the prescribed atmospheric $\delta^{13}C$ curve each time in order to converge on a $\delta^{13}C$ excursion recorded in benthic foraminiferal calcite.

[16] To force the atmosphere in the first model iteration, we adjusted all measured $\delta^{13}C$ values to their atmospheric equivalent, such that the onset of the excursion is set equal to the initial model atmospheric CO_2 $\delta^{13}C$ of −4.9‰ and is held constant beyond 36 kyr after the onset (Figure 3a, black line; supporting information Table S1). We then diagnosed the difference between the $\delta^{13}C$ excursion recorded in a benthic foraminiferal tracer from the model sediment core corresponding to Site 1258, hereafter referred to as 1258′, and the −0.95‰ excursion applied to the atmosphere. We used the model atmosphere-sediment difference to adjust first the shape of the $\delta^{13}C$ excursion applied to the atmosphere (in iteration #2) and then the size (in iteration #3) (for detailed methodology see Appendix A; Figures 3a and 3b). We found that after these 3 iterations, model and data benthic $\delta^{13}C$ were sufficiently similar that further iterations were not required (Figure 3b). The recovered atmospheric $\delta^{13}C$ excursion is then that which generates an excursion in the benthic foraminiferal tracer from 1258′ with the same magnitude and shape as indicated by observations.

[17] We focus here on an iterative series of forcing experiments using a carbon input with an isotopic signature of −25‰ and with bioturbation constant throughout. Carbon with $\delta^{13}C$ of −25‰ is consistent with the oceanic dissolved organic carbon source proposed by *Sexton et al.* [2011] as the driver of the C22r-C21r hyperthermals. However, we also ran

the initial inversion iteration testing carbon sources characterized by isotopic signatures of −60‰ and −12‰, representing methane and a mixture of sources suggested for the PETM carbon release by *Panchuk et al*. [2008] and with and without bioturbational mixing in the sediments (Figure 3c and 3d). (The absence of bioturbation is enacted in the model by setting the biodiffusion coefficient equal to zero throughout the sediment stack.) Obviously, the entire three-part iterative process could be repeated using a carbon input of any specified isotopic composition and with bioturbation turned off. We chose only one particular site for the iterative experiments (1258 and its model equivalent, 1258′) because we have the highest-resolution benthic record from this site; however, it would be possible to conduct the same set of experiments using data from another site, as long as there is approximate match between the model site and the actual site (in terms of paleodepth, sedimentation rate, and wt% $CaCO_3$).

3. Results

[18] Applying a −0.95‰ excursion to the atmosphere with a carbon input of −25‰ results in a −0.62‰ benthic foraminiferal carbon isotope excursion (CIE) in our model analog sediment core to ODP Site 1258 (1258′) (Figures 3a and 3b, black lines). The $\delta^{13}C$ excursion shows a slower onset and an overall longer duration in the sediments relative to the atmosphere. As a result, correcting the atmospheric forcing on the basis of the model atmosphere-sediment difference requires an atmospheric $\delta^{13}C$ excursion that develops more rapidly, occurs over a shorter duration, and has a larger magnitude. By following the three-step iterative method to correct the atmospheric forcing, we converged on a −0.95‰ excursion in benthic foraminiferal $\delta^{13}C$ (Figures 3a and 3b, red lines). The corresponding atmospheric excursion is −1.45‰ and represents our estimate for the true excursion size of event C22nH3. This is associated with a CIE in average surface-dissolved inorganic carbon (DIC) $\delta^{13}C$ in the model of −1.67‰, and −1.56‰ in benthic DIC $\delta^{13}C$ (averaging bottom waters deeper than 2000 m water depth).

[19] While we focus our analysis and discussion on a recovered $\delta^{13}C$ excursion assuming carbon input at −25‰, we also simulated a benthic foraminiferal $\delta^{13}C$ excursion at 1258′ assuming a carbon input of −12‰ and −60‰ (Figure 3c). Compared to the result of inverting the original $\delta^{13}C$ curve and assuming carbon input of −25‰, the −12‰ carbon input generates a sediment excursion that is smaller and with a minimum that is less delayed relative to observations. As a result, recovering the atmospheric CIE with a −12‰ carbon input would result in a slightly larger CIE magnitude with a less abrupt onset. In contrast, the −60‰ carbon input generates a sediment excursion that is larger but with a more delayed minimum, which implies that a slightly smaller CIE with a more abrupt onset would be required to match the observed benthic CIE. Figure 3d demonstrates the difference between the sediment excursion generated with a carbon input of −25‰ and bioturbation "on" (grey line) and the excursion generated with a carbon input of −25‰ and bioturbation "off" (red line) at 1258′. Given that the bioturbation off scenario generates a larger excursion with a less delayed offset, setting bioturbation off during the iterative process would require a smaller CIE with a less abrupt onset compared to the bioturbation on scenario. While we did not repeat the full iterative process using carbon inputs of −60‰ and −12‰ or bioturbation off, the results of these sensitivity experiments provide an indication of how these parameters might change our final result.

4. Discussion

4.1. Backing out the CIE Magnitude

[20] To back out the true CIE, we used a $\delta^{13}C$ record generated from benthic foraminifera rather than from planktonic foraminifera or bulk carbonate. There are several reasons for this. First, the influence on $\delta^{13}C$ of changes in the nannofossil composition of bulk carbonate would be extremely difficult to simulate in a model and equally difficult to validate. Second, planktonic foraminiferal $\delta^{13}C$ can be influenced by a variety of factors such as depth habitat, seasonal variability, and photosymbionts [*Tipple et al*., 2010], again, ecological details that are difficult to simulate in an Earth system model. A carbonate ion effect such as influences planktonic foraminiferal $\delta^{13}C$ [e.g., *Spero et al*., 1997] could be accounted for more easily in cGENIE, but for benthic foraminifera any empirical evidence for such an effect is lacking [*Rathmann and Kuhnert*, 2008]. Moreover, a carbonate ion effect would tend to reduce rather than magnify the recorded excursion, since lower [CO_3^{2-}] as a result of CO_2 input would correspond to heavier $\delta^{13}C$ [*Spero et al*., 1997]. Finally, while both benthic and planktonic foraminifera are subject to diagenesis after burial (or recrystallization and the incorporation of secondary calcite), these factors are likely less significant for benthics owing to their more heavily calcified skeletons [*Tipple et al*., 2010] and closer initial $\delta^{13}C$ values to that of the sedimentary environment. Overall, we consider benthic foraminiferal $\delta^{13}C$ to represent the closest and most robust match between model and observations.

[21] The mismatch between the relative magnitudes of the $\delta^{13}C$ excursion measured in bulk carbonate, benthic foraminifera, and planktonic foraminifera for event C22nH3 compared to simulations in the model support our choice of the benthic foraminiferal record to assess the true size of the CIE (Figure S1). For instance, while the observed benthic foraminiferal CIE from ODP Site 1258 is −0.95‰, the CIE observed in planktonic foraminifera at this site is slightly smaller (−0.83‰) [*Sexton et al*., 2011], and the bulk CIE at this site is smallest (−0.6‰) [*Kirtland Turner*, 2012]. This pattern of relative size is not replicated in the model, where the planktonic foraminiferal tracer records the largest excursion, followed by bulk carbonate, and the benthic foraminiferal tracer records the smallest. Ignoring assemblage changes and vital effects, the greatest modeled excursion occurs in surface ocean DIC as one might expect.

[22] In observations, the smaller magnitude of the excursion in planktonic foraminifera may reflect complications in recording the $\delta^{13}C$ of surface DIC described above. The bulk carbonate CIE recorded in the data is likely the smallest because changes in species composition and thus the apparent fractionation between carbonate and the DIC from which it forms have dampened some of the excursion in a manner that cannot be easily reproduced in a model.

[23] It is possible that the relationship between planktonic and benthic foraminiferal CIE sizes recorded at Site 1258 reflects differences in the size of the excursion in the deep

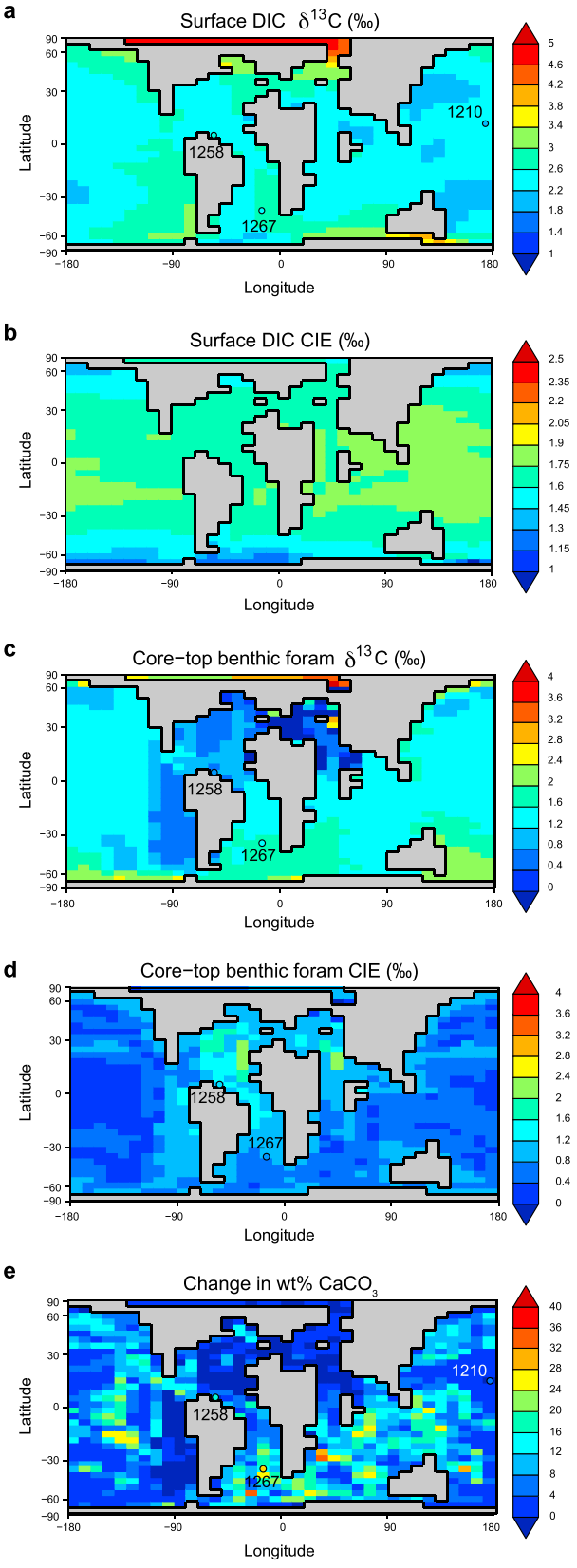

sea compared to the surface ocean. This could suggest changes in ocean circulation or productivity that enhanced the deep-sea magnitude of the event and thus requires some way to evaluate the fidelity of ocean circulation in the model. Benthic $\delta^{13}C$ gradients are primarily driven by (1) the surface $\delta^{13}C$ of sites of deep water formation and (2) the length of the circulation pathway in conjunction with the strength of the biological pump which progressively adds isotopically light carbon. The number of published data points available for this particular interval of the early Eocene is severely limited. We have therefore assessed model bottom water $\delta^{13}C$ (DIC) against benthic foraminiferal $\delta^{13}C$ measurements for a slightly earlier interval and one just prior to the PETM as shown in Figure S2. We obtain a correlation coefficient between observations and equivalent model locations of 0.48, demonstrating some degree of model skill in obtaining the correct sign of the large-scale circulation of the ocean as well as the dominant locations of deep water formation. Model and data agree closely at our key sites—1258 and 1267—as shown in Figure 4c (and Figure S2), giving us some confidence that appropriately sourced water bathes these locations in the model. However, at least in the latest Paleocene, model and data do not agree in the North Atlantic (Figure S2), and the data are consistent with a source of intermediate water that is not reproduced in the model. Any changes in North Atlantic intermediate water formation during C22nH3 could potentially influence Site 1258 and because cGENIE does not predict a North Atlantic intermediate water source, it is possible that the observed $\delta^{13}C$ excursion at 1258 could be amplified by circulation changes, though we have no evidence that this is the case. Finally, it is also possible that C22nH3 was not caused by the propagation of carbon from the atmosphere to the oceans but instead originated in a specific location or water mass. However, the ~1 kyr time scale of mixing of the ocean and CO_2 equilibration with the atmosphere would tend to homogenize the excursion magnitude for an event with an onset time of ~10 kyr. Additional sites sampling across C22nH3, particularly from the Pacific Ocean, are needed to assess whether any pronounced spatial pattern in the CIE exists that cannot be accounted for by sedimentation rate and the other factors discussed in this paper.

[24] The difference in modeled excursion size between atmospheric CO_2 (−1.45‰) and surface DIC (−1.67‰) adds a caveat to the definition of the true CIE magnitude

Figure 4. (a) Distribution of initial surface-dissolved inorganic carbon $\delta^{13}C$ with observations from three sites superimposed. (b) Distribution of the size of the carbon isotope excursion in surface DIC $\delta^{13}C$ when −1.45‰ CIE is applied to the atmosphere. The excursion magnitude ranges from approximately −1.0‰ to −2.0‰. (c) Distribution of initial $\delta^{13}C$ of the benthic foraminiferal tracer in model core tops with observations from two sites superimposed. (d) Distribution of the size of the CIE in the benthic foraminiferal tracer recorded in core-top sediment with observations from two sites superimposed. CIEs range in size from 0.4‰ to >2.0‰. (e) Distribution of the change in modeled sedimentary wt% $CaCO_3$ as a result of the applied −1.45‰ CIE caused by a carbon input with a $\delta^{13}C$ of −25‰ with estimated wt% $CaCO_3$ decreases for three sites superimposed.

for the atmosphere-oceans. The excursion is larger in DIC because of changes in fractionation between dissolved CO_2 and DIC from the onset of the event to the time at which the $\delta^{13}C$ minimum is reached. As the model progressively adds more CO_2 to the atmosphere, surface ocean temperature rises, and excess CO_2 dissolves in the surface ocean, lowering pH and shifting the balance of carbon species in seawater away from the carbonate ion and toward bicarbonate and CO_2. There is a positive fractionation between dissolved CO_2 and DIC that depends on the relative proportion between the different carbon species (CO_2, HCO_3^-, and CO_3^{2-}) as well as temperature (the fractionation scheme during air-sea gas transfer in cGENIE follows that of *Marchal et al*. [1998]) such that fractionation between atmospheric CO_2 and DIC is greater when the proportion of CO_3^{2-} is greater (i.e., before the carbon input). When surface-ocean $[CO_3^{2-}]$ reaches a minimum as a result of the carbon input, the fractionation between atmospheric CO_2 $\delta^{13}C$ and surface DIC $\delta^{13}C$ is reduced, which means that the negative excursion in surface DIC is relatively larger than in atmospheric CO_2. We refer to the atmospheric pCO_2 $\delta^{13}C$ record rather than to the surface DIC record as the true CIE because pCO_2 $\delta^{13}C$ has the advantage of being spatially relatively homogeneous compared to DIC $\delta^{13}C$, which varies regionally as a result of photosynthesis and air-sea gas exchange [*Gruber et al*., 1999; *Lynch-Stieglitz et al*., 1995; *Tipple et al*., 2010] (Figure 4).

4.2. Intersite Differences in Sediment Excursions

[25] Comparison of the CIE record at different model sites allows us to further assess the factors that control the shape of the carbon isotope excursion eventually recorded in the sediments. When pulses of carbon are large enough to cause significant dissolution, they introduce intervals in which it is not possible to record the changing isotopic composition of seawater. Bioturbation can then mask this signal by making it appear that a record is continuous by mixing previously deposited carbonate to the sediment surface [*Panchuk*, 2007; *Ridgwell*, 2007a, 2007b]. In contrast to the severe dissolution at many deep-sea sites across the PETM [e.g. *Zachos et al*., 2005], the smaller CIEs of the Paleogene exhibit less intense dissolution of carbonates throughout the deep sea. For example, at 2000–3000 m, the available records for C22nH3 show that $CaCO_3$ at the peak of the event does not drop below 38 wt%, [*Sexton et al*., 2011]. For this reason, it is likely that the role of dissolution in modifying the recorded signals is comparatively less severe for the smaller Paleogene hyperthermals than for the PETM.

[26] To assess the effect of sedimentation rate on the recorded excursion size, we consider model sediment cores corresponding to two additional sites with sedimentary records through this interval: ODP Site 1210 in the central Pacific (paleodepth ~2000 m) and ODP Site 1267 in the southern Atlantic (paleodepth ~3000 m). Event C22nH3 has been identified from these sites based on estimated wt% $CaCO_3$ data sets [*Sexton et al*., 2011] and corresponds to bulk carbonate $\delta^{13}C$ excursions smaller than that recorded at ODP Site 1258 [*Kirtland Turner*, 2012]. The sediment model grid locations that most closely match these sites are at depths of 2400 m and 3000 m, respectively. Both additional model sites have lower simulated sedimentation rates compared to 1258′ (0.8 cm/kyr at 1210′ and 1.7 cm/kyr at 1267′ compared to 2.5 cm/kyr at 1258′) and higher initial wt% $CaCO_3$, consistent with available data [*Sexton et al*., 2011]. In Figure 5, benthic foraminiferal $\delta^{13}C$ from ODP Site 1267 [*Kirtland Turner*, 2012] shows that our −1.45‰ atmospheric CIE generates a realistic benthic foraminiferal CIE in the model. The benthic foraminiferal CIE recorded in 1267′ and 1210′ is also smaller than 1258′ (Figures 6b–6d, grey lines), consistent with the relationship between bulk stable isotope records [*Kirtland Turner*, 2012].

[27] In addition to the overall magnitude of the CIE, the rate of onset of the excursion and the timing of the isotopic minimum are important factors in the shape of the recorded event. In our experiments, the isotopic minimum is approximately synchronous in surface DIC $\delta^{13}C$ and in the $CaCO_3$ rain flux at all three sites (Figure 6). However, newly preserved $CaCO_3$ mixes with previously buried sediments in the layers below, pushing the signal into older material by bioturbation. As a result, the isotopic minimum within the sediment cores appears consistently earlier than the isotopic minimum in DIC. The relative offset in the timing of the isotopic minimum recorded in model sediment cores is related to the sedimentation rate at each model site—the higher the sedimentation rate, the smaller the impact of "smearing" and so the smaller the lead in the apparent timing of the isotopic minimum compared to DIC (Figure 6). Additionally, the higher sedimentation rate sites show a shorter duration between the onset of the excursion and the isotopic minimum and a shorter overall event compared to the lower sedimentation rate sites. Analagous features are clearly reflected in the ash pulse experiments between bioturbated and non-bioturbated cores and across different sediment rates (Figure 2). Bioturbation also means that the entire excursion appears more dispersed in time in the sediment core compared to DIC (Figure 6).

[28] Differences in the apparent timing of the event have implications for attempts to tune intersite records of CIEs and in determining rates of onset directly from observations. Tuning is typically accomplished by one of two methods—either aligning the peaks at each site or the onsets. Our results suggest that for a given, globally contemporaneous event, records of both the time of onset and time of peak will vary as a function of sedimentation rate (not including any effects of overturning circulation). Aligning records with different sedimentation rates can therefore introduce a few thousand years of error into age models created by assigning an absolute age to an isotopic event. Determining rates of onset directly from the data will lead to an underestimate of the rate of carbon release responsible; with more inaccurate estimates generated from sites with low sedimentation rates (a major problem given that very few Paleogene records have sedimentation rates exceeding 2 cm/kyr).

[29] Assessing modeled intersite differences in the recorded CIE indicates that a caveat to the exercise of recovering the true CIE size is the importance of matching details of the model sites to the data as closely as possible. The model sedimentation rate for 1258′ is probably slightly too high based on age models developed for ODP Site 1258 in this interval [*Sexton et al*., 2006; *Westerhold and Röhl*, 2009], so our true excursion is still a minimum estimate. Sedimentation rate in cGENIE is a function of the fraction of carbonate export from the ocean surface that is preserved together with the applied detrital flux and modified by the bulk composition-dependent porosity [*Ridgwell*, 2007a;

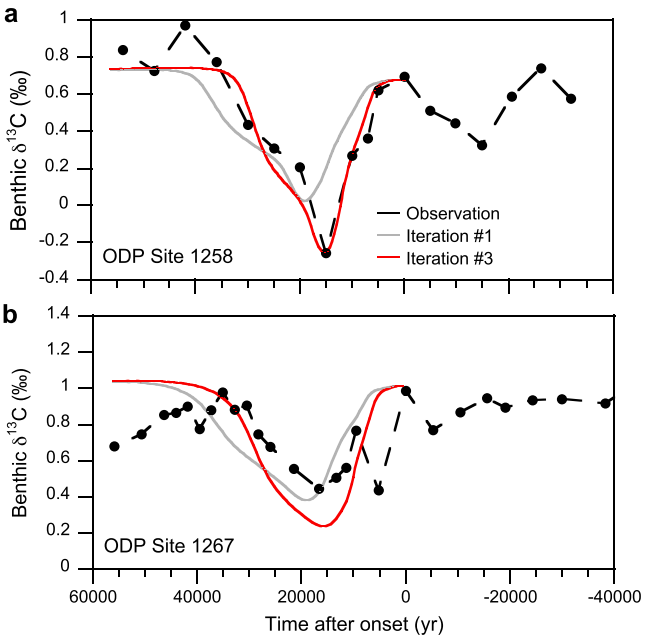

Figure 5. Comparison of model sediment core benthic foraminiferal δ^{13}C results from the initial (grey lines) and final (red lines) inversions to observations (black lines) for (a) ODP Site 1258 [from *Sexton et al.*, 2011], and (b) ODP Site 1267 [*Kirtland Turner*, 2012]. For comparison of the magnitude and timing of CIE between the model and the data, we adjust model-derived values such that the onset of the excursion occurs at the same value as observations and assign time zero as the point at which δ^{13}C values begin to decrease.

Zeebe and Zachos, 2007]. Altering the prescribed detrital flux field (Figure 1) will thus affect the resulting sedimentation rate. The rain ratio of $CaCO_3$ to particulate organic carbon (Figure 1) or the global weathering flux of bicarbonate can also be varied to change the initial wt % $CaCO_3$ [*Panchuk et al.*, 2008]. We do not have nearly as many sites to provide information for the early-middle Eocene as for the late Paleocene [see *Panchuk et al.*, 2008], so our values for the detrital, rain ratio, and weathering parameters are modified from those used for the late Paleocene to best match a relatively small number of data points. Initial conditions at the three model sites that we describe here do not perfectly describe available data, but excessive tuning of model parameters cannot be supported on account of the relatively small number of data points (core sites) available.

[30] Even without a perfect match between model and data site characteristics, our method provides an improved estimate for the size of the CIE suggested by the available sedimentary records. The method can be easily adapted using records from different sites. For instance, benthic data from ODP Site 1267 suggest a negative excursion of ~0.6‰ for C22nH3, in comparison with the −0.95‰ excursion recorded at ODP 1258 [*Kirtland Turner*, 2012]. This is similar to the model difference between the CIE generated in model sediment cores 1258′ and 1267′ (0.95 versus 0.7‰) in response to a −1.45‰ atmospheric CO_2 CIE. The larger difference between the atmospheric CIE and the modeled benthic foraminiferal CIE at model site 1267′ compared to site 1258′ suggests that repeating the iterative exercise using the sediment core 1267′ record would converge on a similar excursion magnitude.

4.3. Diagnosing Carbon Input and Removal

[31] Associated with a −0.95‰ benthic δ^{13}C excursion at model site 1258', atmospheric CO_2 in the model increases from 834 ppm to a peak of 1326 ppm. The total amount of carbon ($\delta^{13}C = -25‰$) added to the atmosphere is 2070 Pg C, with a maximum rate of 0.34 Pg C/yr. In contrast, in the first iteration where the observed and unadjusted benthic foraminiferal CIE is used as the atmospheric δ^{13}C target, the total carbon addition is 1270 Pg with a maximum addition rate of 0.18 Pg/yr (Figures 3e and 3f). The method of recovering the true sediment excursion thus results in a 63% increase in the magnitude of the required carbon input and an 89% increase in the maximum addition rate (Figures 3e and 3f). The diagnosed rate of addition is significantly smaller than that for the PETM assuming a carbon input of the same isotopic composition (~1.7 Pg/yr) [*Cui et al.*, 2011] and considerably smaller than current fossil fuel CO_2 emissions of up to 9.1 Pg C/yr [*Peters et al.*, 2012]. However, it should be recognized that our diagnosed time history of the rate of carbon input and removal is effectively a rolling average. Although we have not explicitly tested it here, a rate of addition of 0.18 Pg/yr over an interval of, e.g., 1 kyr is likely to produce a very similar benthic record to, e.g., a single 100 yr long pulse of 1.8 Pg/yr during that 1 kyr interval. The more frequent the pulses compared to the mixing time of the ocean as well as to that of the bioturbational filter in the sediments, the more difficult it is to distinguish short pulses from a longer-term average, which has important implications for the source and mechanism of carbon release as well as of ocean acidification at the surface [*Hönisch et al.*, 2012].

[32] To fully constrain the overall rate and duration of carbon input during hyperthermal event C22nH3 requires that we can correctly identify the source and hence isotopic composition of the carbon input. We do not have comparable data coverage to constrain the total carbon release against the change in the CCD during this event as in *Panchuk et al.* [2008] for the PETM. However, there is still some value to be gained by contrasting the magnitude of wt% $CaCO_3$ decrease generated in response to our recovered CIE against observational data at the three sites assessed in this study [*Sexton et al.*, 2011] (Figure 4e).

[33] Our model results generally underestimate the magnitude of the wt% $CaCO_3$ decrease, which could be due to inaccurate pre-event wt% $CaCO_3$ or an incorrect isotopic composition for the carbon pulse. In addition, observational records of wt% $CaCO_3$ decrease for C22nH3 at each site are based on estimates interpolated from low-resolution measurements of wt% $CaCO_3$ using high-resolution physical properties data (primarily color reflectance) [*Sexton et al.*, 2011]. It is impossible to generate a perfect model-data fit for these three sites by tuning only global model parameters (i.e., the rain ratio or the weathering flux of bicarbonate), so the initial sedimentary wt% $CaCO_3$ distribution used represents a compromise, with one model site evaluated slightly overestimating observational wt% $CaCO_3$ and the other two underestimating (Figure 1). In order to increase the wt%

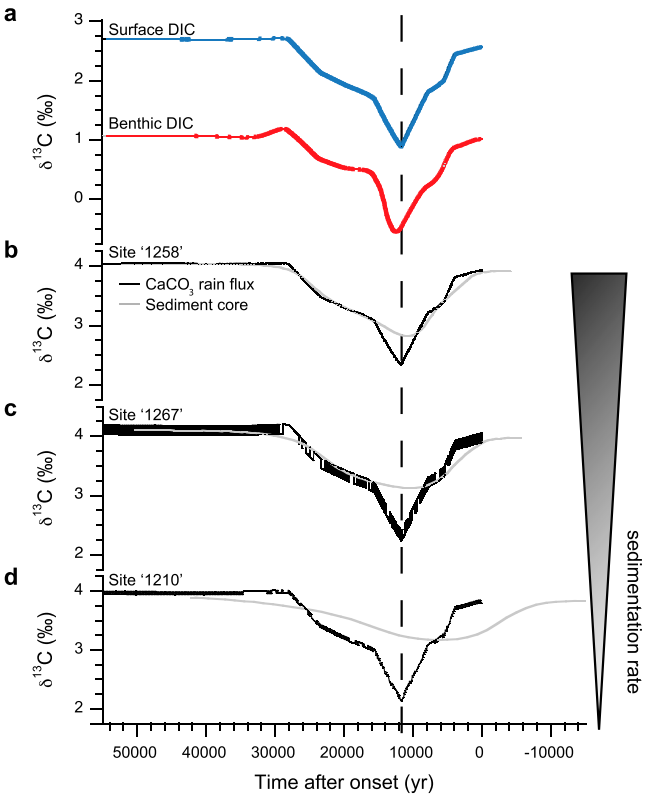

Figure 6. Comparison of the timing of the −1.45‰ atmospheric CIE between (a) surface (blue line) and benthic (red line) DIC, (b) core-top $CaCO_3$ flux (black line) and sediment core (grey line) for model Site 1258′, (c) core-top $CaCO_3$ flux (black line) and sediment core (grey line) for model Site 1267′, and (d) core-top $CaCO_3$ flux (black line) and sediment core (grey line) for model Site 1210′. Dashed line indicates the timing of the $\delta^{13}C$ minimum in surface DIC. The jagged appearance of the $\delta^{13}C$ value of the $CaCO_3$ exported from the ocean surface reflects how the model controls atmospheric $\delta^{13}C$. In this, the model adds or removes a fixed amount of carbon to/from the atmosphere at each model time step such that atmospheric CO_2 $\delta^{13}C$ follows a specified curve (the inversion target). Without using an (unnecessary) involved control algorithm, the simple on/off control means that for each time step, the model may slightly overshoot and have to correct by removing carbon on the subsequent time step. The variations in atmospheric $\delta^{13}C$ are quickly propagated to ocean surface DIC (and hence the $CaCO_3$ flux).

$CaCO_3$ decreases at all model sites, we could (1) decrease the amount of initial wt% $CaCO_3$ or (2) increase the amount of carbon release by choosing a carbon source with a heavier isotopic composition. Given that two of the assessed model sites already underestimate initial wt% $CaCO_3$, the former seems less feasible. Given the latter option, our results suggest that a more depleted carbon source compared to organic carbon (i.e., methane) is unlikely for this particular event. A volcanic emission of carbon of −5‰ is also infeasible, given a required emission of more than 15,000 Pg C, which would result in 0 wt% $CaCO_3$ at a number of model sites where data indicate that wt% $CaCO_3$ remained above 50%. Thus, preliminary model-data comparison suggests a carbon source with $\delta^{13}C$ of −25‰ is a reasonable interpretation.

[34] In order to generate a sediment core CIE with a duration of just 36 kyr, atmospheric CO_2 only stays at its maximum for ~200 years and then begins to decline more rapidly than it rose, with a maximum carbon removal rate reaching 0.4 Pg/yr. Atmospheric CO_2 concentration stabilizes at 730 ppm (lower than the initial concentration). Effectively, it requires a larger perturbation to the carbon cycle to recover from the event than it does to generate it (i.e., the rate of removal is greater than the rate of addition). The maximum rate of carbon removal during the recovery of C22nH3 diagnosed in our experiment is similar to the PETM, at 0.4 Pg/yr [*Cui et al*., 2011]. For the PETM, this asymmetry between the rate of C-input and the rate of removal reflects the long tail of negative $\delta^{13}C$ values recorded for the PETM, with a complete recovery achieved ~150 kyr after the onset [*Cui et al*., 2011]. In our experiment, the rate of removal hits its maximum shortly after the most negative isotopic values are reached (just as in the PETM simulation), but removal of excess carbon is complete by 20 kyr after the event onset (Figures 3e and 3f). In our experiments [as in *Cui et al*., 2011] excess carbon drawdown is not represented by a particular mechanism but is simply a uniform removal in order to match the observed $\delta^{13}C$ record. The diagnosed removal rate may thus have implications for carbon removal processes but does not implicate a particular process such as terrestrial carbon burial or enhanced productivity and marine organic carbon preservation.

4.4. Implications for the Cause of C22nH3

[35] A total carbon release of around 2000 PgC with an organic matter isotopic signature is consistent with the hypothesis of *Sexton et al*. [2011] who posited changes in a highly recalcitrant dissolved organic carbon (DOC) reservoir in the ocean as an explanation for the excursion (albeit *Sexton et al*. [2011] suggested a smaller mass of carbon consistent with interpreting the CIE at face value). Specifically, they proposed that reduced oxygenation of the Eocene ocean may have inhibited the oxidation of fractions of DOC that are today already relatively recalcitrant and allowed a reservoir to build up much larger than the ~600 PgC present in the modern ocean [*Hansell*, 2013]. Oxidizing this pool as a consequence of changes in ocean circulation and hence re-oxygenation of deep waters could explain a decline in $\delta^{13}C$ values associated with events such as C22nH3. Reestablishing the original circulation and reduced oxygenation state would then drive ocean $\delta^{13}C$ back to more positive values as the pool of DOC reestablished. In invoking an ocean circulation driver, a DOC source is consistent with orbital pacing of minor hyperthermals through the early Eocene, perhaps analogous to the mechanism envisioned by *Lunt et al*. [2011].

[36] Problems with the hypothesis surround the mechanism for how a DOC reservoir more than 3 times modern could have built up and then rapidly decayed in response to changes in ocean circulation. Approximately trebling the (modern) inventory to ~2000 PgC would require a two-thirds reduction in its degradation rate—a lifetime of circa 30 kyr. Such a long lifetime would require DOC to be partitioned away from the oxygenated ocean surface in a very substantive stagnation of the deep ocean, yet there is no evidence for pervasive ocean anoxia developing during the Eocene [*Chun et al*., 2010; *Panchuk*, 2007]. However, the rapid rate of carbon removal we

diagnose associated with recovery to pre-event $\delta^{13}C$ values cannot be easily reconciled with silicate-weathering feedback, pointing to the involvement of a dynamic organic carbon subsystem [*Bains et al.*, 2000; *Beerling*, 2000; *Paytan et al.*, 2007; *Bowen and Zachos*, 2010; *Bowen*, 2013].

5. Conclusions

[37] Records of past carbon cycle events recorded in deep-ocean sediments are biased by site-specific preservational effects, but this does not mean that they cannot provide information about the magnitude of the underlying global environmental changes. The cGENIE model, with representations of climate, biogeochemical cycles, and the formation of deep-sea sediment records, allows us to recover an internally (carbon cycle + climate) consistent estimate for the true magnitude of the carbon isotope excursion that characterizes C22nH3 by tracing the various processes that influence recorded CIE size—from the record in the atmosphere to the preserved record in the sediment. The factors influencing the preservation of smaller CIEs, like C22nH3, may be less complicated than for the PETM since dissolution was not nearly as extensive during these events. As a result, it appears that sedimentation rate most strongly influences the details of the excursion recorded at a single site, after accounting for spatial differences in DIC $\delta^{13}C$ due to spatial heterogeneity in productivity and circulation.

[38] Reconstructing ("recovering") the true magnitude of the isotopic excursion in the atmosphere allows us to make improved estimates of the rate and shape of both carbon release and sequestration. Carbon input required to generate these events is much slower than the rate of fossil fuel release due to anthropogenic emissions today and slower than the rate predicted for the PETM as well. As a result, it does not appear that these events are particularly good analogs for the modern in terms of their rate of onset, although their total size would be roughly equivalent to a relatively optimistic scenario of future fossil fuel release, where carbon emissions are kept at about 2000 Pg C.

[39] C22nH3 is not the only hyperthermal event for which biases in the sedimentary record complicate interpretation of the associated carbon cycle dynamics. While potentially more complicated by dissolution and chemical erosion, it may be possible to apply a similar approach to improve estimates for the likely size of the carbon isotopic excursions associated with larger events like Eocene Thermal Maximum-2 or the PETM.

[40] Notably, the rapidity of the recovery from these events is faster than can be explained by ocean uptake and carbonate compensation alone. This information may be useful in constraining models of organic carbon preservation and burial and ultimately help improve the understanding of negative feedbacks that may accelerate the recovery from carbon cycle perturbations, including from the anthropogenic transient.

Appendix A

[41] We calculate the atmospheric $\delta^{13}C$ excursion by means of a three-step process:

[42] 1. Step 1. The atmosphere is forced to follow a −0.95‰ excursion, whose magnitude is taken unadjusted from the benthic $\delta^{13}C$ record of 1258 (Iteration #1).

[43] 2. Step 2. The difference between the time it takes to reach the $\delta^{13}C$ minimum in the atmospheric forcing from Step 1 compared to the time it takes to reach the $\delta^{13}C$ minimum in the Site 1258′ sediment core benthic foraminifera record is assessed. This difference is used to modify the time it takes to reach the $\delta^{13}C$ minimum in the atmospheric forcing. The now modified atmospheric forcing is used to drive a repeat model run—Iteration #2.

[44] 3. Step 3. Using results from Iteration #2, the difference between the magnitude of the $\delta^{13}C$ excursion in the atmosphere compared to the Site 1258′ sediment core benthic foraminifera is now assessed. The difference is used to modify the magnitude of the atmospheric forcing used for a further model run—Iteration #3. In other words, in Iteration #3, both the time it takes to reach the $\delta^{13}C$ minimum and the size of the atmospheric $\delta^{13}C$ excursion have now been adjusted compared to the original forcing of Iteration #1.

[45] The details of the two adjustments carried out to the atmospheric forcings are described below.

[46] We adjust the time it takes to reach the $\delta^{13}C$ minimum (Step 2) by the following:

$$\alpha = \frac{t_{\mathrm{min(atm)}}}{t_{\mathrm{min(sedcore)}}} \tag{A1}$$

where $t_{\mathrm{min(atn)}}$ is the time of the $\delta^{13}C$ minimum in the original forcing (15 kyr), $t_{\mathrm{min(sedcore)}}$ is the time of the $\delta^{13}C$ minimum in the model sediment core response, and α is the scaling factor used to modify the time scale of the forcing applied to the atmosphere in Iteration #2 (Figure 3a, blue line; Iteration #2 in Table S1).

[47] We adjust the magnitude of the forcing (Step 3) by the following:

$$\beta = \frac{\mathrm{CIE_{(atm)}}}{\mathrm{CIE_{(time\text{-}modified\ sedcore)}}} \tag{A2}$$

where $\mathrm{CIE_{(atm)}}$ is the original magnitude of the CIE (0.95‰), $\mathrm{CIE_{(time\text{-}modified\ sedcore)}}$ is the CIE magnitude in the model sediment core from Iteration #2, and β is the factor used to scale the magnitude of the forcing applied to the atmosphere in Iteration #3. The $\delta^{13}C$ excursion applied to the atmosphere in Iteration #3 is our "recovered" or approximated true CIE (Figure 3a, red line). Further iterations of time and CIE magnitude modifications to the $\delta^{13}C$ target could have been carried out. However, we considered the $\delta^{13}C$ profile generated in the Site 1258′ sediment core sufficiently converged toward the observations after a single set of iterations that further sequential ~70 kyr (about 1 week computation on a single-processor core) model experiments were not justified.

[48] Comparing model sediment core composition changes, which are intrinsically a function of depth below the seafloor, with variability recorded in atmosphere and ocean composition (a function of model time), requires that the different records have comparable time scales. Model sediment core $\delta^{13}C$ tracers in cGENIE are saved against $CaCO_3$ age in years before present, such that the greatest age is associated with the onset of the $\delta^{13}C$ excursion. In contrast, the excursion in the atmosphere begins at model time "zero," so for direct comparison between atmospheric CO_2 $\delta^{13}C$ and benthic foraminiferal $\delta^{13}C$ in the model sediment core, we reversed the age scale for the model sediment core. As a result of bioturbation, sediment with a mean $CaCO_3$ age of 55 kyr (equal to the total

experiment duration) is not equivalent to the experiment onset; instead, the onset of the event appears to occur in older material. In order to determine the age of sediment associated with the experiment onset, a pulse of ash was applied to the sediments at the start of each experiment (as per Figure 2). The deepest model sediment core layer containing ash indicates the deepest point to which material dating from the start of the run has mixed, so we assigned this layer as time zero. As a result, we can directly compare the sediment model $\delta^{13}C$ excursions to atmosphere $\delta^{13}C$ excursions.

[49] **Acknowledgments.** This work was supported by an NSF graduate research fellowship and an NSF International Research Fellowship awarded to S. Kirtland Turner, together with a Royal Society University Research Fellowship and NERC grant NE/H023852/1 awarded to A. Ridgwell. S. Kirtland Turner thanks Phil Sexton and Richard Norris for helpful discussions on this topic. The authors also thank Tim Bralower and two anonymous reviewers for comments that improved the text.

References

Archer, D. (1991), Modeling the calcite lysocline, *J. Geophys. Res.*, *96*, 17,037–17,050, doi:10.1029/91JC01812.

Bains, S., R. Norris, R. Corfield, and K. Faul (2000), Termination of global warmth at the Paleocene/Eocene boundary through productivity feedback, *Nature*, *407*, 171–174, doi:10.1038/35025035.

Beerling, D. J. (2000), Increased terrestrial carbon storage across the Palaeocene/Eocene boundary, *Palaeogeogr. Palaeoclimatol. Palaeoecol.*, *161*, 395–400, doi:10.1016/S0031-0182(00)00095-X.

Boudreau, B. P. (1994), Is burial velocity a master parameter for bioturbation?, *Geochim. Cosmochim. Acta*, *58*(4), 1243–1249, doi:10.1016/0016-7037(94)90378-6.

Bowen, G. J. (2013), Up in smoke: A role for organic carbon feedbacks in Paleogene hyperthermals, *Global Planet. Change*, *109*, 18–29, doi:10.1016/j.globplacha.2013.07.001.

Bowen, G. J., and J. C. Zachos (2010), Rapid carbon sequestration at the termination of the Palaeocene-Eocene Thermal Maximum, *Nat. Geosci.*, *3*, 866–869, doi:10.1038/ngeo1014.

Bowen, G. J., D. J. Beerling, P. L. Koch, J. C. Zachos, and T. Quattlebaum (2004), A humid climate state during the Paleocene/Eocene thermal maximum, *Nature*, *432*, 495–499, doi:10.1038/nature03115.

Cao, L., et al. (2009), The role of ocean transport in the uptake of anthropogenic CO_2, *Biogeosciences*, *6*, 375–390, doi:10.5194/bg-6-375-2009.

Chun, C. O. J., M. L. Delaney, and J. C. Zachos (2010), Paleoredox changes across the Paleocene-Eocene Thermal Maximum, Walvis Ridge (ODP Sites 1262, 1263, and 1266): Evidence from Mn and U enrichment factors, *Paleoceanography*, *25*, PA4202, doi:10.1029/2009PA001861.

Colbourn, G., A. Ridgwell, and T. M. Lenton (2013), The Rock Geochemical Model (RokGeM) v0.9, *Geosci. Model Dev.*, *6*, 1543–1573, doi:10.5194/gmd-6-1543-2013.

Corsetti, F. A., A. Baud, P. J. Marenco, and S. Richoz (2005), Summary of Early Triassic carbon isotope records, *C. R. Palevol*, *4*(67), 473–486, doi:10.1016/j.crpv.2005.06.004.

Cramer, B. S., J. D. Wright, D. V. Kent, and M. P. Aubry (2003), Orbital climate forcing of $\delta^{13}C$ excursions in the late Paleocene-early Eocene (chrons C24n-C25n), *Paleoceanography*, *18*(4), 1097, doi:10.1029/2003PA000909.

Cui, Y., L. R. Kump, A. J. Ridgwell, A. J. Charles, C. K. Jinium, A. F. Diefendorf, K. H. Freeman, N. M. Urban, and J. C. Harding (2011), Slow release of fossil fuel carbon during the Paleocene-Eocene Thermal Maximum, *Nat. Geosci.*, *4*, 481–485, doi:10.1038/ngeo1179.

DeConto, R. M., S. Galeotti, M. Pagani, D. Tracy, K. Schaefer, T. Zhang, D. Pollard, and D. J. Beerling (2012), Past extreme warming events linked to massive carbon release from thawing permafrost, *Nature*, *484*, 87–91, doi:10.1038/nature10929.

Dickens, G. R., J. O'Neil, D. Rea, and R. Owen (1995), Dissociation of oceanic methane hydrate as a cause of the carbon isotope excursion at the end of the Paleocene, *Paleoceanography*, *10*, 965–971, doi:10.1029/95PA02087.

Dickens, G. R., M. M. Castillo, and J. C. G. Walker (1997), A blast of gas in the latest Paleocene: Simulating first-order effects of massive dissociation of oceanic methane hydrate, *Geology*, *25*(3), 259–262, doi:10.1130/0091-7613(1997)025<0259:ABOGIT>2.3.CO;2.

Dunkley Jones, T., A. Ridgwell, D. J. Lunt, M. A. Maslin, D. N. Schmidt, and P. J. Valdes (2010), A Palaeogene perspective on climate sensitivity and methane hydrate instability, *Philos. Trans. R. Soc. A*, *368*(1919), 2395–2415, doi:10.1098/rsta.2010.0053.

Galeotti, S., S. Krishnan, M. Pagani, L. Lanci, A. Gaudio, J. C. Zachos, S. Monechi, G. Morelli, and L. Lourens (2010), Orbital chronology of Early Eocene hyperthermals from the Contessa Road section, central Italy, *Earth Planet. Sci. Lett.*, *290*(1-2), 192–200, doi:10.1016/j.epsl.2009.12.021.

Gibbs, M. T., G. J. S. Bluth, P. J. Fawcett, and L. R. Kump (1999), Global chemical erosion over the last 250 Myr: Variations due to changes in paleogeography, paleoclimates, and paleogeology, *Am. J. Sci.*, *299*, 611–651, doi:10.2475/ajs.299.7-9.611.

Gibbs, S. J., P. R. Bown, B. H. Murphy, A. Sluijs, K. M. Edgar, H. Palike, C. T. Bolton, and J. C. Zachos (2012), Scaled biotic disruption during early Eocene global warming events, *Biogeosciences*, *9*, 4679–4688, doi:10.5194/bgd-9-1237-2012.

Gruber, N., C. D. Keeling, R. B. Bacastow, P. R. Guenther, T. J. Lueker, M. Wahlen, H. A. J. Meijer, W. G. Mook, and T. F. Stocker (1999), Spatiotemporal patterns of carbon-13 in the global surface oceans and the oceanic Suess effect, *Global Biogeochem. Cycles*, *13*, 307–335, doi:10.1029/1999GB900019.

Handley, L., P. N. Pearson, I. K. McMillan, and R. D. Pancost (2008), Large terrestrial and marine carbon and hydrogen isotope excursions in a new Paleocene/Eocene boundary section from Tanzania, *Earth Planet. Sci. Lett.*, *275*, 17–25, doi:10.1016/j.epsl.2008.07.030.

Hansell, D. (2013), Recalcitrant dissolved organic carbon fractions, *Annu. Rev. Mar. Sci.*, *5*, 421–445, doi:10.1146/annurev-marine-120710-100757.

Heinze, C. (2001), Towards the time dependent modeling of sediment core data on a global basis, *Geophys. Res. Lett.*, *28*, 4211–4214, doi:10.1029/2001GL013479.

Higgins, J. A., and D. P. Schrag (2006), Beyond methane: Towards a theory for the Paleocene–Eocene Thermal Maximum, *Earth Planet. Sci. Lett.*, *245*(3–4), 523–537, doi:10.1016/j.epsl.2006.03.009.

Holden, P. B., N. R. Edwards, S. A. Miller, K. I. C. Oliver, R. M. Death, and A. Ridgwell (2013), Controls on the spatial distribution of oceanic $\delta^{13}C_{DIC}$, *Biogeosciences*, *10*, 1815–1833, doi:10.5194/bg-10-1815-2013.

Hönisch, B., et al. (2012), The geological record of ocean acidification, *Science*, *335*(6072), 1058–1063, doi:10.1126/science.1208277.

Hull, P. M., P. J. S. Franks, and R. D. Norris (2011), Mechanisms and models of iridium anomaly shape across the Cretaceous-Paleogene boundary, *Earth Planet. Sci. Lett.*, *301*(1-2), 98–106, doi:10.1016/j.epsl.2010.10.031.

John, C. M., S. M. Bohaty, J. C. Zachos, A. Sluijs, S. Gibbs, H. Brinkhuis, and T. J. Bralower (2008), North American continental margin records of the Paleocene Eocene thermal maximum: Implications for global carbon and hydrological cycling, *Paleoceanography*, *23*, PA2217, doi:10.1029/2007PA001465.

Kirtland Turner, S. (2012), High-resolution paleoceanography and modeling of abrupt warming events on greenhouse Earth, Ph.D. Dissertation, University of California, San Diego, La Jolla, CA. [Available at http://escholarship.org/uc/item/05v3p9xs.]

Kump, L. R., T. J. Bralower, and A. Ridgwell (2009), Ocean acidification in deep time, *Oceanography*, *22*(4), 94–107, doi:10.5670/oceanog.2009.100.

Kurtz, A. C., L. R. Kump, M. A. Arthur, J. C. Zachos, and A. Paytan (2003), Early Cenozoic decoupling of the global carbon and sulfur cycles, *Paleoceanography*, *18*(4), 1090, doi:10.1029/2003PA000908.

Lourens, L. J., A. Sluijs, D. Kroon, J. C. Zachos, E. Thomas, U. Röhl, J. Bowles, and I. Raffi (2005), Astronomical pacing of late Palaeocene to early Eocene global warming events, *Nature*, *435*, 1083–1087, doi:10.1038/nature03814.

Lunt, D. J., A. Ridgwell, A. Sluijs, J. C. Zachos, S. Hunter, and A. Haywood (2011), Orbital pacing of methane hydrate destabilization during the Paleogene, *Nat. Geosci.*, *4*, 775–778, doi:10.1038/ngeo1266.

Lynch-Stieglitz, J., T. F. Stocker, W. S. Broecker, and R. G. Fairbanks (1995), The influence of air-sea exchange on the isotopic composition of oceanic carbon: Observations and modeling, *Global Biogeochem. Cycles*, *9*, 653–665, doi:10.1029/95GB02574.

Magioncalda, R., C. Dupuis, T. Smith, E. Steurbaut, and P. D. Gingerich (2004), Paleocene-Eocene carbon isotope excursion in organic carbon and pedogenic carbonate: Direct comparison in a continental stratigraphic section, *Geology*, *32*(7), 553–556, doi:10.1130/G20476.1.

Marchal, O., T. F. Stocker, and F. Joos (1998), A latitude-depth, circulation biogeochemical ocean model for paleoclimate studies: Development and sensitivities, *Tellus, Ser. B*, *50*(3), 290–316, doi:10.1034/j.1600-0889.1998.t01-2-00006.x.

Mook, W. G. (1986), ^{13}C in atmospheric CO_2, *Neth. J. Sea Res.*, *20*, 211–223.

Nunes, F., and R. D. Norris (2006), Abrupt reversal in ocean overturning during the Palaeocene/Eocene warm period, *Nature*, *439*, 60–63, doi:10.1038/nature04386.

Pagani, M., K. Caldeira, D. Archer, and J. C. Zachos (2006a), An ancient carbon mystery, *Science*, *314*, 1556–1557, doi:10.1126/science.1136110.

Pagani, M., et al. (2006b), Arctic hydrology during global warming at the Palaeocene/Eocene thermal maximum, *Nature*, *442*, 671–675, doi:10.1038/nature05043.

Panchuk, K. (2007), Investigating the Paleocene/Eocene Carbon Cycle Perturbation: An Earth System Model Approach, PhD dissertation, The Pennsylvania State University.

Panchuk, K., A. Ridgwell, and L. R. Kump (2008), Sedimentary response to Paleocene-Eocene Thermal Maximum carbon release: A model-data comparison, *Geology*, *36*(4), 315–318, doi:10.1130/G24474A.1.

Paytan, A., K. Averyt, K. Faul, E. Gray, and E. Thomas (2007), Barite accumulation, ocean productivity, and Sr/Ba in barite across the Paleocene-Eocene Thermal Maximum, *Geology*, *35*(12), 1139–1142, doi:10.1130/G24162A.1.

Peng, T.-H., W. S. Broecker, and W. H. Berger (1979), Rates of benthic mixing in deep-sea sediment as determined by radioactive tracers, *Quat. Res.*, *11*(1), 141–149, doi:10.1016/0033-5894(79)90074-7.

Peters, G. P., G. Marland, C. Quéré, T. Boden, J. G. Canadell, and M. R. Raupach (2012), Rapid growth in CO_2 emissions after the 2008–2009 global financial crisis, *Nat. Clim. Change*, *2*, 2–4, doi:10.1038/nclimate1332.

Rathmann, S., and H. Kuhnert (2008), Carbonate ion effect on Mg/Ca, Sr/Ca and stable isotopes on the benthic foraminifera Oridorsalis umbonatus off Namibia, *Mar. Micropaleontol.*, *66*(2), 120–133, doi:10.1016/j.marmicro.2007.08.001.

Ridgwell, A. (2001), Glacial-interglacial perturbations in the global carbon cycle, PhD thesis, University of East Anglia at Norwich, Norwich, U. K.

Ridgwell, A. (2007a), Interpreting transient carbonate compensation depth changes by marine sediment core modeling, *Paleoceanography*, *22*, PA4102, doi:10.1029/2006PA001372.

Ridgwell, A. (2007b), Application of sediment core modeling to interpreting the glacial-interglacial record of Southern Ocean silica cycling, *Clim. Past*, *3*, 387–396. [Available at www.clim-past.net/3/387/2007.]

Ridgwell, A., and J. C. Hargreaves (2007), Regulation of atmospheric CO_2 by deep-sea sediments in an Earth system model, *Global Biogeochem. Cycles*, *21*, GB2008, doi:10.1029/2006GB002764.

Ridgwell, A., and D. N. Schmidt (2010), Past constraints on the vulnerability of marine calcifiers to massive carbon dioxide release, *Nat. Geosci.*, *3*, 196–200, doi:10.1038/ngeo755.

Ridgwell, A., and R. E. Zeebe (2005), The role of the global carbonate cycle in the regulation and evolution of the Earth system, *Earth Planet. Sci. Lett.*, *234*(3–4), 299–315, doi:10.1016/j.epsl.2005.03.006.

Ridgwell, A., I. Zondervan, J. C. Hargreaves, J. Bijma, and T. M. Lenton (2007), Assessing the potential long-term increase of fossil fuel uptake due to CO_2-calcification feedback, *Biogeosciences*, *4*, 481–492. [Available at www.biogeosciences.net/4/481/2007.]

Ruddiman, W. F., G. A. Jones, T.-H. Peng, L. K. Glover, B. P. Glass, and P. J. Liebertz (1980), Tests for size and shape dependency in deep-sea mixing, *Sediment. Geol.*, *25*, 257–276, doi:10.1016/0037-0738(80)90064-0.

Schiffelbein, P. (1984), Effect of benthic mixing on the information content of deep-sea stratigraphical signals, *Nature*, *311*, 651–653, doi:10.1038/311651a0.

Schouten, S., M. Woltering, W. Irene, C. Rijpstra, A. Sluijs, H. Brinkhuis, and J. S. Sinninghe Damsté (2007), The Paleocene–Eocene carbon isotope excursion in higher plant organic matter: Differential fractionation of angiosperms and conifers in the Arctic, *Earth Planet. Sci. Lett.*, *258*(3–4), 581–592, doi:10.1016/j.epsl.2007.04.024.\.

Sexton, P. F., P. A. Wilson, and R. D. Norris (2006), Testing the Cenozoic multisite composite $\delta^{18}O$ and $\delta^{13}C$ curves: New monospecific Eocene records from a single locality, Demerara Rise (Ocean Drilling Program Leg 207), *Paleoceanography*, *21*, PA2019, doi:10.1029/2005PA001253.

Sexton, P. N., R. D. Norris, P. A. Wilson, H. Palike, T. Westerhold, U. Rohl, C. T. Bolton, and S. Gibbs (2011), Multiple Eocene 'hyperthermal' events driven by ocean ventilation, *Nature*, *471*, 349–353, doi:10.1038/nature09826.

Sluijs, A., and G. R. Dickens (2012), Assessing offsets between the $\delta^{13}C$ of sedimentary components and the global exogenic carbon pool across early Paleogene carbon cycle perturbations, *Global Biogeochem. Cycles*, *26*, GB4005, doi:10.1029/2011GB004224.

Smith, C. R., and C. Rabouille (2002), What controls the mixed-layer depth in deep-sea sediment? The importance of POC flux, *Limnol. Oceanogr.*, *47*(2), 418–426, doi:10.4319/lo.2002.47.2.0418.

Spero, H. J., J. Bijma, D. W. Lee, and B. E. Bemis (1997), Effect of seawater carbonate concentration on foraminiferal carbon and oxygen isotopes, *Nature*, *390*, 497–500, doi:10.1038/37333.

Thomas, D. J., J. C. Zachos, T. J. Bralower, E. Thomas, and S. Bohaty (2002), Warming the fuel for the fire: Evidence for the thermal dissociation of methane hydrate during the Paleocene-Eocene thermal maximum, *Geology*, *30*, 1067–1070.

Thomas, E., and J. C. Zachos (2000), Was the late Paleocene thermal maximum a unique event?, in *Early Paleogene Warm Climates and Biosphere Dynamics*, GFF—Stockholm Geological Society Transactions, vol. 122, edited by B. Schmitz et al., pp. 169–170, Taylor and Francis, London, U.K.

Tindall, J., R. Flecker, P. Valdes, D. N. Schmidt, P. Marwick, and J. Harris (2010), Modelling the oxygen isotope distribution of ancient seawater using a coupled ocean-atmosphere GCM: Implications for reconstructing early Eocene climate, *Earth Planet. Sci. Lett.*, *292*(3-4), 265–273, doi:10.1016/j.epsl.2009.12.049.

Tipple, B. J., S. R. Meyers, and M. Pagani (2010), Carbon isotope ratio of Cenozoic CO_2: A comparative evaluation of available geochemical proxies, *Paleoceanography*, *25*, PA3202, doi:10.1029/2009PA001851.

Trauth, M. H. (1998), TURBO: A dynamic-probabilistic simulation to study the effects of bioturbation on paleoceanographic time series, *Comput. Geosci.*, *24*(5), 433–441, doi:10.1016/S0098-3004(98)00019-3.

Trauth, M. H., M. Sarnthein, and M. Arnold (1997), Bioturbational mixing depth and carbon flux at the seafloor, *Paleoceanography*, *12*, 517–526, doi:10.1029/97PA00722.

Westerhold, T., and U. Rohl (2009), High resolution cyclostratigraphy of the early Eocene—New insights into the origin of the Cenozoic cooling trend, *Clim. Past*, *5*, 309–327, doi:10.5194/cp-5-309-2009.

Zachos, J. C., et al. (2005), Rapid acidification of the ocean during the Paleocene-Eocene Thermal Maximum, *Science*, *308*(5728), 1611–1615, 10.1126/science.1109004.

Zachos, J. C., S. M. Bohaty, C. M. John, H. McCarren, D. C. Kelly, and T. Nielson (2007), The Paleocene-Eocene carbon isotope excursion: Constraints from individual shell planktonic foraminifer records, *Philos. Trans. R. Soc. A*, *365*, 1829–1842, doi:10.1098/rsta.2007.2045.

Zachos, J. C., H. McCarren, B. Murphy, U. Röhl, and T. Westerhold (2010), Tempo and scale of late Paleocene and early Eocene carbon isotope cycles: Implications for the origin of hyperthermals, *Earth Planet. Sci. Lett.*, *299*(1–2), 242–249, doi:10.1016/j.epsl.2010.09.004.

Zeebe, R. E., and J. C. Zachos (2007), Reversed deep-sea carbonate ion basin gradient during Paleocene-Eocene thermal maximum, *Paleoceanography*, *22*, PA3201, doi:10.1029/2006PA001395.

Zeebe, R. E., J. C. Zachos, and G. R. Dickens (2009), Carbon dioxide forcing alone insufficient to explain Palaeocene—Eocene Thermal Maximum warming, *Nat. Geosci.*, *2*, 576–580, doi:10.1038/ngeo578.